Manifold Alignment with Schroedinger Eigenmaps

Juan E. Johnson[a], Charles M. Bachmann[b], and Nathan D. Cahill[a]

[a]Center for Applied and Computational Mathematics, School of Mathematical Sciences, Rochester Institute of Technology, Rochester, NY 14623, USA
[b]Chester F. Carlson Center for Imaging Science, Rochester Institute of Technology, Rochester, NY 14623, USA

ABSTRACT

The sun-target-sensor angle can change during aerial remote sensing. In an attempt to compensate BRDF effects in multi-angular hyperspectral images, the Semi-Supervised Manifold Alignment (SSMA) algorithm pulls data from similar classes together and pushes data from different classes apart. SSMA uses Laplacian Eigenmaps (LE) to preserve the original geometric structure of each local data set independently. In this paper, we replace LE with Spatial-Spectral Schoedinger Eigenmaps (SSSE) which was designed to be a semisupervised enhancement to the to extend the SSMA methodology and improve classification of multi-angular hyperspectral images captured over Hog Island in the Virginia Coast Reserve.

Keywords: Manifold Alignment, Domain Adaption, Hyperspectral Images, Classification

1. INTRODUCTION

The remote sensing field has progressed rapidly with the inclusion of very high resolution (VHR) hyperspectral images (HSI) as new orbital satellites come online.[1] Multimodal remote sensing allows for many views of the same region of interest (ROI). Using a single sensor for analysts limits inferences and generalizations of classification schemes used on that ROI. This is because the analysis of a ROI is limited by the acquisition parameters such as sun elevation, sun-target-sensor angle and atmospheric conditions. By incorporating more information like multiview, multiband, multisensor, or multitemporal images for data, a more complete model of a ROI can be obtained.

Ground truth acquisition campaigns can be expensive in the remote sensing community; however good labeled instances are essential for producing robust classification and target detection machine learning methods. It is unfortunate but one cannot simply incorporate previous campaign labeled information from an old ROI into a newly updated ROI despite the two ROIs sharing very similar spatial locations. Variations in vegetation, composition, soil moisture, topography, and illumination conditions lead to spectral variability.[2] This is especially true for the case of multitemporal data which creates the need for fusion schemes like domain adaption for multimodal hyperspectral data.[1]

This paper attempts to build on the domain adaption approach to multimodal remote sensing by leveraging ideas from manifold alignment.[3] Manifold alignment is a framework that fuses source domains (in this case two HSIs) and creates a target domain (a new latent space) where the geometry of the original manifolds are preserved, the similarities between the source domains are pushed together and the dissimilarities between the source domains are pushed apart. Tuia et al.[4] used a method called semisupervised manifold alignment (SSMA) which attempts to use labeled samples from each source domain in order to achieve manifold alignment of multimodal hyperspectral remotely sensed images. By using a few labeled samples from each domain a connectivity graph is created for each image. The Laplacian graph is constructed to preserve the geometry for the individual manifolds of each image. This is akin to the Laplacian eigenmaps (LE) scheme[5] which is one of the pivotal approaches to nonlinear dimensionality reduction.

Further author information: (Send correspondence to J.E.J.)
J.E.J.: jej2744@rit.edu
C.M.B.: bachmann@rit.edu
N.D.C.: nathan.cahill@rit.edu

One extension is the Schroedinger eigenmaps[6] (SE) approach which enhances the Laplacian graph by means of a potential matrix. This potential term is flexible in its use and has been shown to be useful for classification[7] and target detection[8][9] of hyperspectral images. Further extensions of this method have shown that this potential term can be used to incorporate spatial information of the remote sensing scene to enhance the classification accuracy of the hyperspectral image[10].[11] In the case of Indian Pines and the IEEE GRSS 2013 Data Fusion Contest dataset, there is evidence that using some preprocessing techniques like superpixels, random projections and randomized singular value decomposition schemes can mitigate the computational burden of the graph construction and eigenvalue decomposition[12].[13] In this context, the inclusion of a SE potential matrix as the geometric preserving term for classification of HSI is explored. The rest of this paper is organized as follows: Section 2 - The mathematical preliminaries of semisupervised manifold alignment are described. Section 3 - The geometry preserving term is explored with the Laplacian matrix and the addition of the potential matrix. Section 4 describes the data used and classification experiments created. Section 5 shows the results of the classification experiments. Section 6 illustrates the conclusions drawn from the experiments and discusses future efforts.

2. SEMISUPERVISED MANIFOLD ALIGNMENT (SSMA)

The method proposed by Wang et al.[14] is used to align separate data manifolds from their respective source domains by projecting them into a common target space or a joint latent space $\mathcal{F}$. The objective was to preserve the local geometry of the data from each source domain as well as bring similar regions together in the target domain whilst pushing dissimilar regions apart in the target domain. The projection functions are found for each data manifold. Tuia et al.[4] applied this methodology to hyperspectral images of varying degrees of angle of acquisition. They were able to achieve better classification accuracy after performing semisupervised manifold alignment than if they were to just classify each image separately or together without any alignment methodology.

2.1 Notation

This particular problem assumes that we have two hyperspectral data sets, but this method can be extended to M data sets of any nature. Each data set, $\mathbf{X}_m \in \mathbb{R}^{d_m}$ where $m = 1, 2$, has a set of labeled sample pairs $\{x_j^m, y_j^m\}_{j=1}^{l_s}$ and unlabeled samples $\{x_i^m\}_{i=1}^{u_s}$ where $l_m << u_m$. We construct a matrix $\mathbf{X}_m$ by incorporating labeled and unlabeled samples. Furthermore, we can construct a block diagonal data matrix $\mathbf{X} \in \mathbb{R}^{d \times N}$ which has of all X_m matrices, where $d = \sum_{m=1}^{M} d_m$ and $N = \sum_{n=1}^{M} n_m$. Tuia et al. notes that it is possible to have images of different spatial and spectral resolution so it is possible that $d_m \neq d'_m$. The term domain is a general term used to describe the space we are operating on. So the two source domains would be the original independent HSI and the target domain would be the final embedding that encompasses information from both source domains.

2.2 Semisupervised Loss Function

Wang et al. wanted to align M datasets into a common representation by constructing M mapping functions to the latent space $\mathcal{F}$. So we want a mapping function $f^m \in \mathbb{R}^{d_m \times d}$ that projects dataset $\mathbf{X}_m$ into the latent space $\mathcal{F}$. Tuia et al.[4] would like similar classes from each image domain to be close together in the latent space $\mathcal{F}$ while dissimilar classes in the latent space $\mathcal{F}$ are further apart. This formulation results in minimizing the distance between the similar classes whilst maximizing the distance between the dissimilar classes. Wang et al.[3] reduced this problem to solving a standard Rayleigh quotient cost function to be minimized:

$$\mathbf{C}_{opt} = \underset{F}{\operatorname{argmin}} \frac{\mathbf{F^T X(L_s + \mu L_g) X^T F}}{\mathbf{F^T X L_d X^T F}} \quad , \tag{1}$$

where $\mathbf{F}$ is a d by d projection matrix. The row blocks of this matrix correspond to the d_m by d projection functions for each m domain for source domain $\mathbf{X}_m$. The term $\mathbf{L_s} + \mu\mathbf{L_g}$ is minimized by solving the cost function whereas the term $\mathbf{L_d}$ is maximized by solving the cost function. $\mathbf{L_s}$ represents the similarities between the classes between domains augmented by the individual geometric structure of each source domain, $\mathbf{L_g}$ where μ is a tradeoff parameter between the two affinity matrices. $\mathbf{L_d}$ represents the distances that we want maximized between source domains in the latent space. The next section describes the construction of said graph Laplacian matrices.

2.3 Similarity, Dissimilarity and Geometric Terms

2.3.1 Laplacian Eigenmaps and Locality Preserving Projections

The Laplacian matrix L_g ensures that the individual manifold geometry for each source domain is preserved in the target domain. This is constructed in the same manner as the Laplacian Eigenmaps (LE) algorithm.[5] This motivation for using this form is its computational efficiency, its locality preservation in high dimensional space, and its relationship to popular spectral cluster methods such as ratio cuts[15] and normalized cuts.[16] It involves the following three main steps:

1. Construct an undirected graph $\mathcal{G} = (\mathcal{X}, \mathcal{E})$ where $\mathcal{X}$ are the data points that represent the vertices of graph $\mathcal{G}$, and $\mathcal{E}$ represents the proximity between each vertex $\mathcal{X}$.
2. Define the weights for the edges $\mathcal{E}$.
3. Compute the smallest $k+1$ eigenvalues and eigenvectors of the generalized eigenvalue problem $\mathbf{Lf} = \lambda\mathbf{Df}$, where $\mathbf{D}$ is the degree matrix of the weighted adjacency matrix $\mathbf{W}$ defined as $D_{ii} = \sum_j W_{i,j}$ and $\mathbf{L} = \mathbf{D} - \mathbf{W}$ is the Laplacian matrix. The ordered eigenvectors $\mathbf{f}_0, \ldots, \mathbf{f}_k$ for the k smallest nontrivial eigenvalues is the optimal embedding for the lower dimensional space.

The LE algorithm gives us the flexibility to define different edges and edge weights when we construct our affinity matrix. One common way is to use the heat kernel defined as the weighted $W_{ij} = e^{\frac{-||x_i - x_j||^2}{\sigma}}$ matrix if an edge exists between data points x_i and x_j or $W_{ij} = 0$ otherwise.

The linearized counterpart to the LE algorithm is the Locality Preserving Projections (LPP) scheme.[17] Explicit projection functions to map any point from the source embedding to the target embedding. LPP has the same construction as the LE scheme except for the final generalized eigenvalue problem becomes $\mathbf{XLX^T f} = \lambda\mathbf{XDX^T f}$ where $\mathbf{X}$ is the matrix of all the data points in the original space. The ordered eigenvectors $\mathbf{f}_1, \ldots, \mathbf{f}_k$ are the solutions and the embedding $\mathbf{y}_i$ can be found from $\mathbf{F}^T\mathbf{x}$ where $\mathbf{F} = (\mathbf{f}_1, \ldots, \mathbf{f}_k)$. This method has advantages over LE because it yields a simple, linear algorithm that is defined everywhere. It also provides computational improvements and has the ability to be kernelized to provide a nonlinear extension.

2.3.2 Geometric Preservation

The geometric preserving term $\mathbf{L_g}$ is constructed using the heat kernel on the k-NN graph for each domain separately, $\mathbf{L_g^m}$. So each source domain laplacian matrix $\mathbf{L_g^m} = \mathbf{D_g^m} - \mathbf{W_g^m}$ were $\mathbf{D_g^m}$ is the degree matrix defined as $D_g^m(ii) = \sum_j W_g^m(ij)$. The laplacian matrix is constructed for each individual source domain and then put into a block matrix for the $\mathbf{L_g}$ term.

2.3.3 Similarity Preservation

The $\mathbf{L_s}$ similarity term is to bring the similar samples closer together in the target domain. An adjacency matrix, $\mathbf{W_s}$ is constructed based on the class similarities or correspondence. The matrix, $\mathbf{W_s}$ has a 1 if the samples have the same label and a 0 otherwise. The laplacian matrix, $\mathbf{L_s^m} = \mathbf{D_s^m} - \mathbf{W_s^m}$ is constructed where $\mathbf{D_s^m}$ is the degree matrix defined as $D_s^m(ii) = \sum_j W_s^m(ij)$.

2.3.4 Dissimilarity Preservation

The L_d dissimilarity term is to push the dissimilar samples further apart in the target domain. An adjacency matrix, $\mathbf{W_d}$ is constructed based on the class dissimilarities or opposition. The matrix $\mathbf{W_d}$ has a 1 if the samples have different labels and a 0 otherwise. The Laplacian matrix, $\mathbf{L_d^m} = \mathbf{D_d^m} - \mathbf{W_d^m}$ is constructed where $\mathbf{D_d^m}$ is the degree matrix defined as $D_d^m(ii) = \sum_j W_d^m(ij)$.

2.4 Generalized Eigenvalue Problem

The solution to the optimization function proposed in 1 is given by the following generalized eigenvalue problem:

$$\mathbf{X}(\mathbf{L}_s + \mu\mathbf{L}_g)\mathbf{X}^T\gamma = \lambda\mathbf{X}\mathbf{L}_d\mathbf{X}^T\gamma \ . \tag{2}$$

By finding the eigenvectors γ_i corresponding to the smallest eigenvalues, we can find projection functions for each source domain to the target domain as defined by the row blocks

$$\gamma = [\mathbf{f_1}, \mathbf{f_2}, \ldots, \mathbf{f_{d_{max}}}] = \begin{bmatrix} \mathbf{f_1^1}, \mathbf{f_2^1}, \ldots, \mathbf{f_{d_{max}}^1} \\ \mathbf{f_1^2}, \mathbf{f_2^2}, \ldots, \mathbf{f_{d_{max}}^2} \end{bmatrix} \ . \tag{3}$$

Each block within the γ contains the M projection functions needed to project the data from the source domain $\mathbf{X_m}$ to the latent space $\mathcal{F}$ which projection function $\mathbf{f}_m$. We can project the data from one domain to another by:

$$\mathbf{P}_{\mathcal{F}}(\mathbf{X_i}) = \mathbf{f_i^T}\mathbf{X_i} \ . \tag{4}$$

Furthermore, we can project any data sample from a domain m to another domain m' by using the psuedoinverse and that can be written as:

$$\mathbf{P_i}(\mathbf{X_j}) = (\mathbf{f_j}\mathbf{f_i^\dagger})^\mathbf{T}\mathbf{X_j} \ . \tag{5}$$

2.5 Properties and Benefits

Tuia et al.[4] outline a number of benefits to this method for multimodal hyperspectral remote sensing.

- *Projection Functions* - this method defines explicit projection functions that map large data from their source domain to a latent space target domain.
- *Multisensor* - this method exploits the geometry of each source domain exclusively. This implies that there are no restrictions on the number of bands needed per HSI nor the properties of the HSI.
- *Multidomain* - this method can align an arbitrary number of domains into a common latent space. They found that there was no need for the leading source domains to have any alignment in their spectral resolutions.
- *PDF-based* - this method aligns the PDFs of the image sources without needing spatially coregistered images.
- *Invertibility* - since this method computes explicit projection functions, one utilizes the pseudoinverse to project all images from their respective source domains to an explicit source domain of choice and not necessarily just the target domain.

3. SCHROEDINGER EIGENMAPS FOR MANIFOLD ALIGNMENT

3.1 Schroedinger Eigenmaps

SE is an enhancement of the well established LE spectral clustering routine. The SE method works by enhancing the graph Laplacian in the LE routine via a barrier or a cluster potential. By incorporating expert/labeled information on a subset of pixels, the user can encode this expert knowledge into the LE methodology as a semisupervised learning method.

3.2 Potential Term

Czaja[6] generalizes the LE method by introducing a potential term, $\mathbf{V}$, on the graph Laplacian, $\mathbf{L}$. So the Laplacian operator on the graph is replaced by the following Schroedinger operator:

$$\mathbf{S} = \mathbf{L} + \alpha\mathbf{V} \ . \tag{6}$$

The traditional LE algorithm results in the generalized eigenvalue problem again. By including the potential term, $\mathbf{V}$, the new generalized eigenvalue problem is given by:

$$(\mathbf{L} + \alpha\mathbf{V})\mathbf{f} = \lambda\mathbf{D}\mathbf{f} \ , \tag{7}$$

and solving for the k smallest eigenvalues to extract their corresponding eigenvectors for the new embedding. If using the cluster potential methodology, V is also a Laplacian graph except the construction of the adjacency matrix is given by expert user knowledge. In the context of HSI classification, one could incorporate expert knowledge in the form of class similarities or spatial locations.

3.2.1 Spatial-Spectral Fusion

There have been many attempts to incorporate spatial information into the LE methodology for HSI classification. This can be done by constructing heat kernels that combined the spatial and spectral information. Cahill et al.[10] successfully constructed a cluster potential matrix that would encode the proximity between the spatial components of the vertices. This was able to increase the classification accuracy of the Indian Pines image. The cluster potential was constructed like so:

$$\mathbf{V} = \sum_{i=1}^{k} \sum_{\mathbf{x}_j \in \mathcal{N}_\epsilon^p(\mathbf{x}_i)} \mathbf{V}(i,j)\omega_{i,j} e^{-\frac{||x_i^p - x_j^p||^2}{\sigma_p^i}} \ , \tag{8}$$

where $\mathcal{N}_\epsilon^p(\mathbf{x}_i)$ is the set of points in the ϵ-neighborhood of $\mathcal{X}$, $\omega(i,j) = e^{-\frac{||x_i^f - x_j^f||^2}{\sigma_f^2}}$, and $V(i,j)$ can be defined as:

$$V(i,j)_{k,l} = \begin{cases} 1, & (k,l) \in \{(i,i),(j,j)\} \\ -1, & (k,l) \in \{(i,j),(j,i)\} \\ 0, & \text{otherwise} \end{cases} \ . \tag{9}$$

The $\mathbf{V}(i,j)$ term incorporated the spectral information of the pixels and One distinct advantage of the SSSE methodology is the ability to change the impact of the spatial-spectral information by the use of the parameter α or by the $\omega(i,j)$.

3.3 New Cost Function

As this potential matrix is defined, the SE algorithm proceeds in the same way as the LE except we are minimizing a different cost function than the SSMA method. Furthermore, our final cost function for the manifold alignment algorithm is defined as:

$$\mathbf{F}_{opt} = \underset{F}{\operatorname{argmin}} \frac{\mathbf{F^T X}(\mathbf{L_s} + \mu(\mathbf{L_g} + \alpha\mathbf{V}))\mathbf{X^T F}}{\mathbf{F^T X L_d X^T F}} \ . \tag{10}$$

We end up solving the following eigenvalue decomposition

$$\mathbf{X}(\mathbf{L_s} + \mu(\mathbf{L_g} + \alpha\mathbf{V}))\mathbf{X^T}\gamma = \lambda\mathbf{X}\mathbf{L_d}\mathbf{X^T}\gamma \ . \tag{11}$$

where the only visible change is the included potential term $\mathbf{V}$ to augment the geometric term $\mathbf{L_g}$.

3.4 Hypothesis

The SSSE method has demonstrated that its competitive with standard state-of-the-art spectral-spatial fusion approaches for spectral clustering and hyperspectral image classification. Incorporating spatial and spectral information has shown to be a useful technique to increase classification accuracies for hyperspectral imagery. By incorporating this enhancement to the SSMA methodology, there should be an increase in classification accuracy of the latent space. This should be especially true in images with higher spatial resolutions as opposed to images with a higher spectral resolution.

4. CLASSIFICATION EXPERIMENTS

4.1 Data

We use a HSI dataset provided by Virgnia Commonwealth University which covers the Hog Island region of the Virginia Coast Reserve (VCU).[18] There are two images in question. The first image was captured at an altitude of 2000m above the site with 96 spectral bands. The second image was captured at 400m above the site with 48 spectral bands. A subset of both images has been obtained that are georeferenced to the same datum. Both images have been partially labeled with 1927 and 802 ground truth pixels respectively associated with 7 classes.

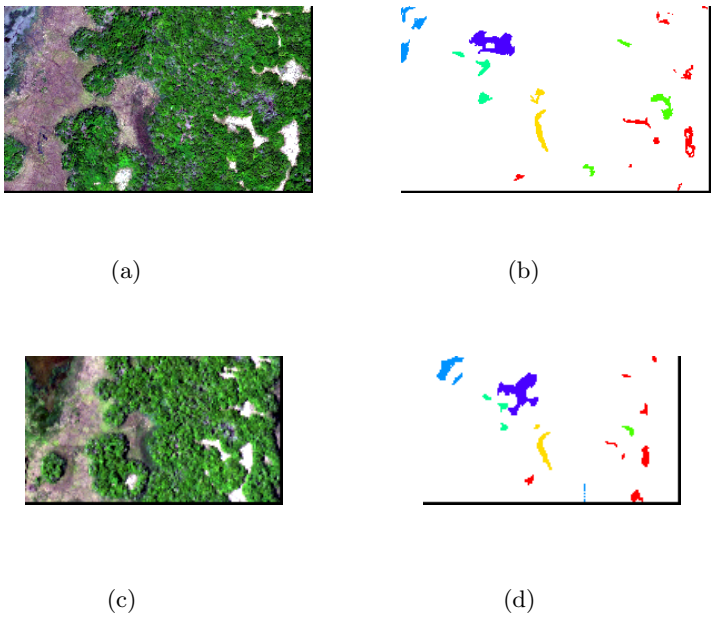

(a) (b)

(c) (d)

Figure 1: Original subset image 1 and and ground truth: (a) Subset Image 1 (ENVI True Color Approximation), (b) Subset Image 1 ground truth, (c) Subset Image 2, (ENVI True Color Approximation), (d) Subset Image 2 ground truth.

4.2 Experimental Setup

We compare SSMA with the proposed SSMA with the SSSE potential matrix by performing the manifold alignment on the two HSI (two independent domains) and then subsequently perform classification on the latent space. The classification step is performed using linear discriminant analysis (LDA) as implemented in MATLAB with 20% of each class selected from the ground truth pixels from the two HSI subsets. A percent of the training samples were to be used as labeled samples with the remaining percent of samples to be used as unlabeled samples. We present four cases to study the effect of the potential matrix on the SSMA method. Case 1 has randomly selected 40% labeled samples for domain 1 and domain 2. Case 2 has randomly selected 20% and 10% labeled samples samples for domain 1 and domain 2 respectively. Case 3 has randomly selected 20% and 40%

labeled samples for domain 1 and 2 respectively. Case 4 has randomly selected 40% and 10% labeled samples for domain 1 and 2 respectively. The remaining percent of samples were used as unlabeled samples for each domain and case. We repeated the classification 10 times and computed the average overall accuracy (OA) (via the κ coefficient) the average accuracy (AA), the average precision (AP), and the average specificity (ASp) with respect to each dimension for the final embedding. Each statistic was compared and contrasted for both domains and for all cases. The OA is the result chosen to be displayed in this paper.

Prior to the dimensionality reduction step, the spectral components of the data $\mathcal{X}$ were normalized so that $(1/k)\sum_{i=1}^{k}||\mathbf{x}_i^f||_2 = 1$. Note that while this type of normalization is fine when performing experiments on a single image, it is not appropriate to apply independently to different images when comparing classification results across a set of images. This is because the magnitudes of the spectral components of the data carry useful class-specific information that can be distorted or lost when different images are normalized differently. The intial choice of parameters are $\sigma_f = \sigma_p = 1$ for the SSSE method and the parameters are adjusted when necessary to improve performance. For all manifold alignment algorithms, we reduced the dimension up to 1/3 of the original dimension and performed classification on every dimension. For all graph construct steps in any algorithm, a k value of 20 was used. For the SSSE algorithm, the parameter α was chosen based on the suggestion in Cahill et. al.[10]

5. RESULTS

5.1 Parameter Estimation, μ

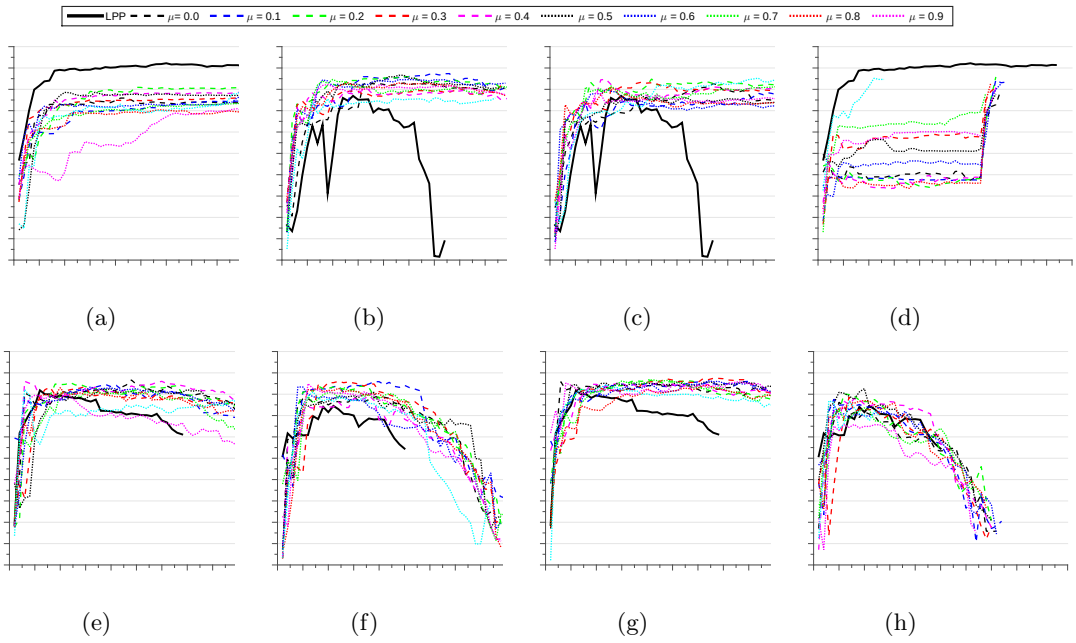

Figure 2: Overall accuracy (OA) for different values of μ compared to the LPP implementation for each source domain. The values range between 0 and 1. The x-axis represents the number of dimensions used for classification. The values range between 0 and 50 dimensions. (a), (b), (c), and (d) are for Domain I. (e), (f), (g) and (h) are for Domain II.

The results in figure 2 represent the OA or κ statistic with respect to the number of dimensions used for the classification. The different values of μ (the trade off parameter for the SSMA method) are shown with different line colors and styles. The four cases with the respective μ values are also outlined above. Case 1 has a decrease in OA for domain 1 whereas there is an increase in OA for domain 2. Case 2 shows an increase in OA for domain 1 and domain 2. Case 3 shows an increase in OA for both domains. Case 4 has an increase in classification

accuracy for domain 2 but a decrease in classification accuracy for domain 1. From this experiment, it appears that the spectral domain can get an increase in OA despite the limited number of samples present. However, a lower spectral resolution might have a decrease in OA regardless of the number of samples present in domain 1. This may be because the spectral resolution has a large effect on the latent space domain as it is shown in all cases.

Table 1: This table gives the μ and α values chosen for each domain that produced the best overall classification accuracy.

Cases	Domain I			Domain II		
	μ_1	α_1	α_2	μ_2	α_1	α_2
I	0.5	0.46	4.64	0.4	100	2.15
II	0.1	46.42	1.00	0.3	2.15	46.42
III	0.4	21.54	10.00	0.3	0.46	21.54
IV	0.6	0.22	0.22	0.5	0.1	0.1

5.2 Parameter Estimation, α

With the best values of μ chosen in table 1, these were compared to different values of α for adding the spatial-spectral potential. The objective of this experiment was to try and get α values that would increase the OA of the SSMA methodology. Figure 3 gives α_1 and α_2 values that maximized the OA of the first and second domain respectively. In case 1 for α_1, there is not a major increase in classification accuracy until the number of dimensions reaches 25 where $\alpha_1 = 0.46$ obtains κ coefficient of 0.8. However, $\alpha_2 = 0.2$ gives a higher OA of 0.8 at around the 9th dimension. For domain 2, there is an increase in classification accuracy for multiple values of α_1 up to a κ coefficient of 0.87. This is a similar case for α_2 which results in a κ coefficient up to 0.89. This makes a minimal difference compared to the standard LPP method because there are a large number of labeled samples present. However, there is an increase in OA for the second domain despite the limited number of samples present.

For the first domain, case 2 does not have a significant increase in OA for α_1 values. However, there is an accuracy increase for α_2 values compared with the maximum μ_2 value. The knowledge transfer could be higher or the geometric component of the potential could have increased the effectiveness of the SSMA method. The second domain shows an increase of OA with multiple α_1 values but only in the earlier dimensions. The α_2 values all have a greater OA compared to the μ_2 value chosen but not much of a greater OA compared to the μ_1 value chosen.

When there are a limited number of samples involved, domain 1 seems to have a greater increase in OA with the additional potential matrix. Case 3 shows that there is no increase in the OA for domain 1 regardless of the α value to trade off the potential matrix. There are still a small number of samples for domain 2 so there is still an increase in the OA for some α_1 and α_2 values up to a κ coefficient of 0.89.

The last case supports the notion that a low number of samples from an image with higher spectral resolution can decrease the classification accuracy of an image with a lower spectral resolution that has more samples. Case 1 has a higher number of samples for the higher spectral resolution whereas case 4 has a lower number of samples. One possible explanation is the complexity of the spectral materials is not captured with a lower number of samples. The latent space does not seem to capture the inherent nature of both target domains. The potential matrix does increase the OA for domain 1 on case 4 which is due to the nearest spatial neighbours but the LPP has the best OA. Conversely, the large number of samples does increase the OA for the higher spectral domain but the potential matrix does not increase the OA compared to the SSMA.

Figure 4 gives the maximum OA for μ and α values. Many samples available for both domains do not necessarily increase the OA for the high spatial and high spectral domains. The general LPP method can obtain good OA results for domain 1 but the SSMA method can reach better OA for domain 2. The additional potential term does not have better OA than the SSMA method until more dimensions are included.

Case 2 shows that the maximum values of μ for both domains get higher OA than the standard LPP method. However, the potential matrices can get higher OA for both domains for fewer dimensions for domain 1 and

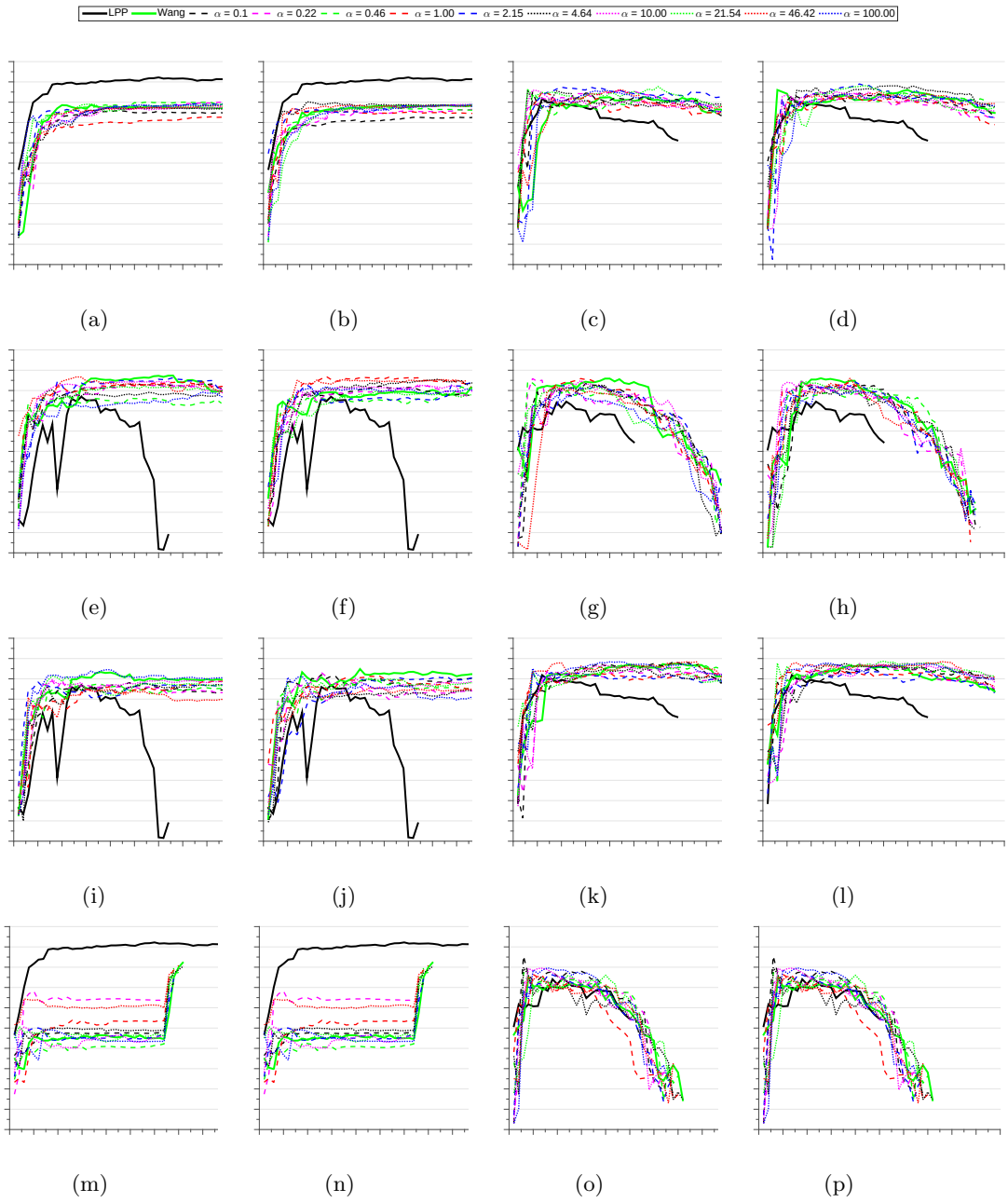

Figure 3: Overall accuracy (OA) for different values of α_1 (the α value that maximized the OA for the first domain) compared to the LPP implementation for each source domain. The values range between 0 and 1. The x-axis represents the number of dimensions used for classification. The values range between 0 and 50 dimensions. (a), (b), (c), and (d) are for Case I. (e), (f), (g), and (h) are for Case II. (i), (j), (k), and (l) are for Case III. (m), (n), (o), and (p) are for Case IV.

and domain 2. This is a very similar to case 3 for the first domain where there are limited number of samples. However, the abundance of samples for cases 1 and 3 for the second domain do not show much increase in OA for μ or α values. Case 4 highlights the decrease in OA with μ and α values for domain 1. It is worth mentioning that there are areas where the OA is higher or similar with the addition of the potential term consistently for

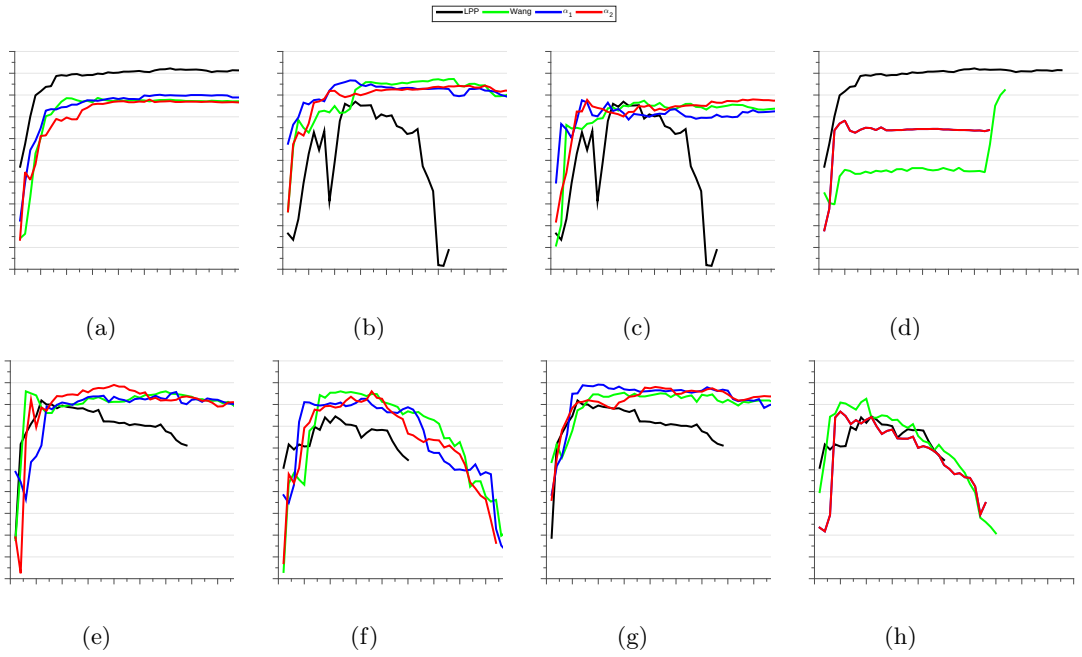

Figure 4: Overall accuracy (OA) and the associated value of α and μ. The values range between 0 and 1. The x-axis represents the number of dimensions used for classification. The values range between 0 and 50 dimensions. (a), (b), (c), and (d) are for Domain I. (e), (f), (g) and (h) are for Domain II.

all of the cases except for case 4.

6. CONCLUSIONS AND DISCUSSION

In this article, we proposed an enhancement to the existing class of manifold alignment algorithms by taking advantage of the spatial information present in the HSI. This algorithm is based onthe SSSE method which was designed to be a semisupervised enhancement to the traditional LE algorithm. By constructing a graph using spectral and spatial information present in the image via a cluster potential, we can bring together samples geometrically which should preserve the inherent structure of the source domain. Classification experiments on the Hog Island dataset show that the proposed method of manifold alignment on the HSI image with a higher spectral resolution exhibited an improved OA in certain cases. The image with a higher spatial resolution showed a higher OA only when there were a limited number of samples available from both domains. The spectral dimension showed the most improvement for OA as the potential matrix was able to highlight certain geometries within the subspace. One possible fault of this formulation is the neglect of the scaling term $\mathbf{D}$ in the generalized eigenvalue problem. The addition of the potential term gives an arbitrary scaling to certain vertices without highlighting the important vertices via the diagonal matrix, $\mathbf{D}$.

REFERENCES

[1] Gomez-Chova, L., Tuia, D., Moser, G., and Camps-Valls, G., "Multimodal Classification of Remote Sensing Images: A Review and Future Directions," *Proceedings of the IEEE* **103**, 1560–1584 (sep 2015).

[2] Yang, H. L. and Crawford, M. M., "Spectral and Spatial Proximity-Based Manifold Alignment for Multi-temporal Hyperspectral Image Classification," *IEEE Transactions on Geoscience and Remote Sensing* **54**, 51–64 (jan 2016).

[3] Wang, C., Krafft, P., and Mahadevan, S., [*Manifold Alignment*], 1 ed. (2011).

[4] Tuia, D., Volpi, M., Trolliet, M., and Camps-Valls, G., "Semisupervised manifold alignment of multimodal remote sensing images," *IEEE Transactions on Geoscience and Remote Sensing* **52**(12), 7708–7720 (2014).

[5] Belkin, M. and Niyogi, P., "Laplacian eigenmaps and spectral techniques for embedding and clustering.," *NIPS* (2001).

[6] Czaja, W. and Ehler, M., "Schroedinger eigenmaps for the analysis of biomedical data," *IEEE Transactions on Pattern Analysis and Machine Intelligence* **35**, 1274–1280 (may 2011).

[7] Benedetto, J., Czaja, W., Dobrosotskaya, J., Doster, T., Duke, K., and Gillis, D., "Semi-supervised learning of heterogeneous data in remote sensing imagery," in [*Independent Component Analyses, Compressive Sampling, Wavelets, Neural Net, Biosystems, and Nanoengineering X*], Szu, H. and Dai, L., eds., **8401**, 840104–840104–12 (may 2012).

[8] Dorado Munoz, L. P., Messinger, D. W., and Czaja, W., "Assessment of Schrodinger Eigenmaps for target detection," in [*Algorithms and Technologies for Multispectral, Hyperspectral, and Ultraspectral Imagery XX*], Velez-Reyes, M. and Kruse, F. A., eds., 908813 (jun 2014).

[9] Dorado-Munoz, L. P. and Messinger, D. W., "Schrodinger Eigenmaps for spectral target detection," in [*Algorithms and Technologies for Multispectral, Hyperspectral, and Ultraspectral Imagery XXI*], Velez-Reyes, M. and Kruse, F. A., eds., **9472**, 947211 (may 2015).

[10] Cahill, N. D., Czaja, W., and Messinger, D. W., "Schroedinger Eigenmaps with nondiagonal potentials for spatial-spectral clustering of hyperspectral imagery," in [*Algorithms and Technologies for Multispectral, Hyperspectral, and Ultraspectral Imagery XX*], Velez-Reyes, M. and Kruse, F. A., eds., 908804 (jun 2014).

[11] Cahill, N. D., Chew, S. E., and Wenger, P. S., "Spatial-spectral dimensionality reduction of hyperspectral imagery with partial knowledge of class labels," in [*Algorithms and Technologies for Multispectral, Hyperspectral, and Ultraspectral Imagery XXI*], **9472**, 94720S (2015).

[12] Zhang, X., Chew, S. E., Xu, Z., and Cahill, N. D., "SLIC Superpixels for Efficient Graph-Based Dimensionality Reduction of Hyperspectral Imagery," in [*Algorithms and Technologies for Multispectral, Hyperspectral, and Ultraspectral Imagery XXI*], **9472**, 947209 (2015).

[13] Czaja, W., Hafftka, A., Manning, B., and Weinberg, D., "Randomized Approximations of Operators and their Spectral Decomposition for Diffusion Based Embeddings of Heterogeneous Data," in [*Compressed Sensing Theory and its Applications to Radar, Sonar and Remote Sensing (CoSeRa)*], 75–79 (2015).

[14] Wang, C. and Mahadevan, S., "Heterogeneous domain adaptation using manifold alignment," *IJCAI International Joint Conference on Artificial Intelligence* , 1541–1546 (2011).

[15] Chan, P. K., Schlag, M., and Zien, J., "Spectral K -Way Ratio-Cut Partitioning Part I : Preliminary Results," *IEEE Transactions on Computer-Aided Design of Integrated Circuits and Systems* **13**(9), 1088 – 1096 (1992).

[16] Jianbo Shi and Malik, J., "Normalized cuts and image segmentation," *IEEE Transactions on Pattern Analysis and Machine Intelligence* **22**(8), 888–905 (2000).

[17] He, X. and Niyogi, P., "Locality preserving projections," *Neural information processing systems* **16**, 153 (2004).

[18] "Hyperspectral imagery for Hog Island, VA, 2013." http://www.vcrlter.virginia.edu/cgi-bin/showDataset.cgi?docid=knb-lter-vcr.229 (2013). [Online; accessed 6-April-2016].